Y. Xie and C. T.-C. Nguyen, "A low-voltage tiltable microplatform using bent-beam actuation" *Tech. Digest*, 2002 Solid-State Sensor, Actuator, and Microsystems Workshop, Hilton Head, South Carolina, June 2-6, 2002, pp. 350-353.

A LOW-VOLTAGE TILTABLE MICROPLATFORM USING BENT-BEAM ACTUATION

Yuan Xie and Clark T.-C. Nguyen
Center for Integrated Microsystems
Department of Electrical Engineering and Computer Science
University of Michigan
Ann Arbor, Michigan 48109-2122, U.S.A.

ABSTRACT

A tiltable microplatform for adaptive artificial vision applications has been demonstrated that utilizes special bent-beam electrostatic actuators to achieve DC tilt angles larger than 10^o with actuation voltages less than 20V, and a resonance tilt angle of 19^o when driven to resonance at 33 kHz via a combination of 14V DC, plus 5V AC. This bent-beam actuation mechanism has the further advantage that its physical implementation is out of the way of the microplatform itself, making it amenable to applications where light must pass through the platform and substrate (e.g., adaptive vision).

Keywords: MOEMS, artificial vision, tilt angle, low voltage

I. INTRODUCTION

In the wake of rapid advancements in optical MEMS technology spurred by the telecommunications industry, micromechanical actuation mechanisms capable of generating plate tilt angles on the order of 10^o are now commonplace [1]-[3]. Among the various actuation strategies, vibromotor [1] and bimorph [2] methods stand out as some of the most voltage efficient, requiring 20V AC and 1-2 V (but with considerable power consumption), respectively, to attain tilt angles greater than 10^o in large plates, often for optical scanning applications. However, actuation methods capable of low power, low voltage tilt actuations of plates that allow light to pass through a 3D array of elements are fewer in number [3], and most require excessive power or voltage levels.

One such 3D arrayed application, for which this work is specifically targeted, is the adaptive artificial vision system depicted in Fig. 1, where incoming light is collected, subdivided into a 2D array, collimated, then directed through an array of tiltable microprisms before finally reaching a pixel array. In this system, the microprisms disperse the color content of the incoming light, and by tilting, modulate the colors from pixel to pixel on the detection plane—an operation often required by algorithms for color adaptation in vision systems [4]. Because the change in the angle of light passing through a prism is only a weak function of the prism tilt, tilt angles of 10^o or greater are needed for adequate traversal of colors over adjacent pixels, and such tilts must be accomplished via low voltages and with low power consumption.

This paper describes a new bent-beam electrostatic (i.e., low power) actuation method that achieves DC platform tilts larger than 10^o with actuation voltages less than 20V and resonance tilts up to 19^o at 33 kHz, while offering an implementation structure amenable to applications requiring 3D arrayed transmission-based operation.

II. MICROPLATFORM OPERATION

Figure 2 presents a perspective-view schematic of the demonstrated tiltable microplatform housing a microprism. As shown, the low-stress nitride microplatform itself is suspended via rigid polysilicon suspension beams above a hole in the silicon substrate (as in [3]) that (1) allows light to pass through; and (2) allows unimpeded tilting of the microplatform over very large angles. The suspension beams are actually not anchored to the substrate directly, but rather rest upon the substrate via strategically-placed dimples, around which the suspensions can pivot to affect tilting of the platform. These pivoting suspension beams together with the network of

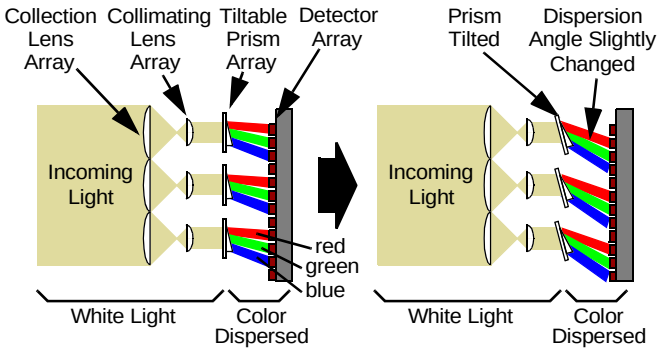

Fig. 1: Schematic of a portion of the adaptive artificial vision application targeted by the tiltable microplatform. Beyond the detector array, vision algorithms are applied to the 2D data via transistor DSP circuits, then fed back to control platform tilting so as to affect color adaptation.

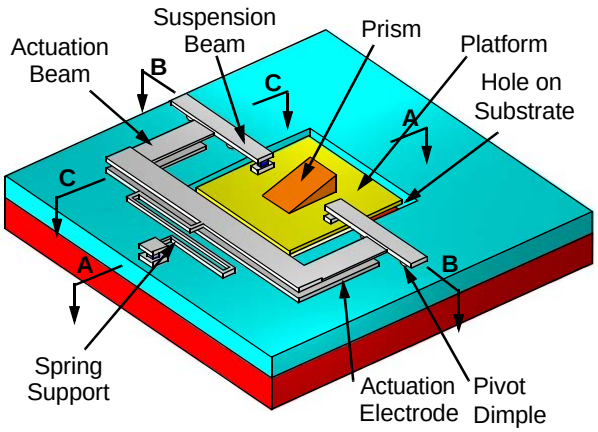

Fig. 2: 3D view of the bent-beam actuated tiltable microplatform

beams attached to them then realize the bent-beam actuation mechanism that makes possible tilting of the platform at such low voltages. As illustrated in Fig. 3, bent-beam actuation is achieved by pulling down a thin doped-polysilicon beam perpendicularly attached to the suspension beam, and bending this thin beam close to the suspension dimple so as to pivot the suspension around an angle defined by the degree of bending in the thin beam. In this work, the thin beam is pulled down electrostatically by applying a suitable voltage to an underlying, nitride-covered (to prevent shorting), doped-polysilicon electrode. The voltage required to achieve a given angle is greatly reduced in this system, because: (1) the pivoting dimple eliminates the need to overcome a torsional stiffness; and (2) once pulled down, portions of the beam near the bend are very close to the underlying electrode, so the electrostatic beam-bending force is larger for a given voltage.

III. BENT-BEAM ACTUATOR DESIGN

To obtain an expression for tilt angle as a function of applied actuation voltage for a bent-beam actuator, an energy method similar to that described in [5] is used, in which the derivative of the total potential energy in the system with respect to distance is set to

Travel support has been generously provided by the Transducers Research Foundation and by the DARPA MEMS and DARPA BioFlips programs.

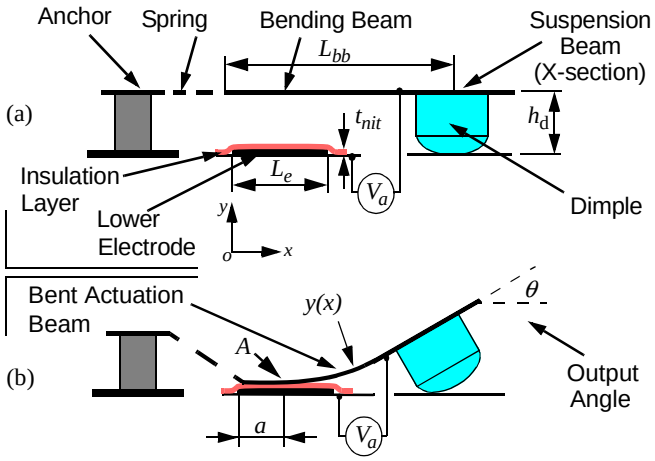

Fig. 3: Schematics describing the mechanism behind bent-beam actuation. (a) Before and (b) after application of the actuation voltage V_a.

zero at equilibrium.

Using this technique, neglecting fringing electric fields and dimple-to-substrate friction, the voltage required to pin the bending beam up to the point *A* in Fig. 3 can be derived and written as

$$V_a(a) = \sqrt{\frac{(12h_d^2 EI)/(L_{bb}-a)^4}{\frac{\varepsilon_{nit}\varepsilon_o W_{bb}}{t_{nit}} + \frac{\varepsilon_o W_{bb}\delta z(a)}{\delta a}}} \qquad (1)$$

where

$$z(a) = (L_{bb}-a)\sqrt{\frac{\varepsilon_{nit}}{h_d t_{nit}}} \cdot \operatorname{atan}\left[(L_e-a)\sqrt{\frac{\varepsilon_{nit}h_d}{t_{int}(L_{bb}-a)^2}}\right] \qquad (2)$$

and where L_{bb} and W_{bb} are the length and the width, respectively, of the bending beam, L_e is the length of the actuation electrode, a is the electrode-to-beam contact length when the bending beam is pinned to the substrate, h_d is the height of the dimple, t_{nit} is the thickness of the insulation layer, E is the Young's modulus of polysilicon, I is the bending moment of the bending beam, ε_{nit} is the dielectric constant of the insulation layer, and ε_o is the permittivity of free space. Using (1) to determine the distance a generated by a given voltage V_a, the tilt angle can then be determined via the expression

$$\theta(a) = \operatorname{atan}\left[\frac{dy(x)}{dx}\right]\Bigg|_{x=L_{bb}} = \operatorname{atan}\left[\frac{2h_d}{L_{bb}-a}\right] \qquad (3)$$

where $y(x)$ is the deflection of the beam, approximately parabolic.

IV. FABRICATION PROCESS

The fabrication process for the tiltable microplatform combines surface micromachining with deep RIE and phased lithography, and is very briefly summarized in Fig. 4. The process begins with the growth of a 2μm thermal oxide insulation layer, which is patterned to form sealant vias that later prevent etching of the isolation layer during a final HF release etch step. 1μm of silicon rich (low stress) LPCVD nitride is then deposited at 835°C to fill the sealant vias and to serve as the structural material for the eventual microplatform. Next, 3000Å of LPCVD polysilicon is deposited at 588°C, then $POCl_3$-doped and patterned to form electrodes and electrical interconnect. An 1800Å layer of stoichiometric nitride is then deposited and patterned over the patterned polysilicon to serve as an insulation layer that prevents shorting between the actuation electrodes and suspended polysilicon structures (c.f., Fig. 3). The platform nitride is then patterned and covered by a 3.3μm-thick LPCVD high temperature oxide (HTO) layer, deposited at 920°C, that sets the gap spacing between the actuation electrodes and the bending beams. Next, 3000Å of LPCVD polysilicon is deposited at 588°C, then doped and patterned to form the bending beams.

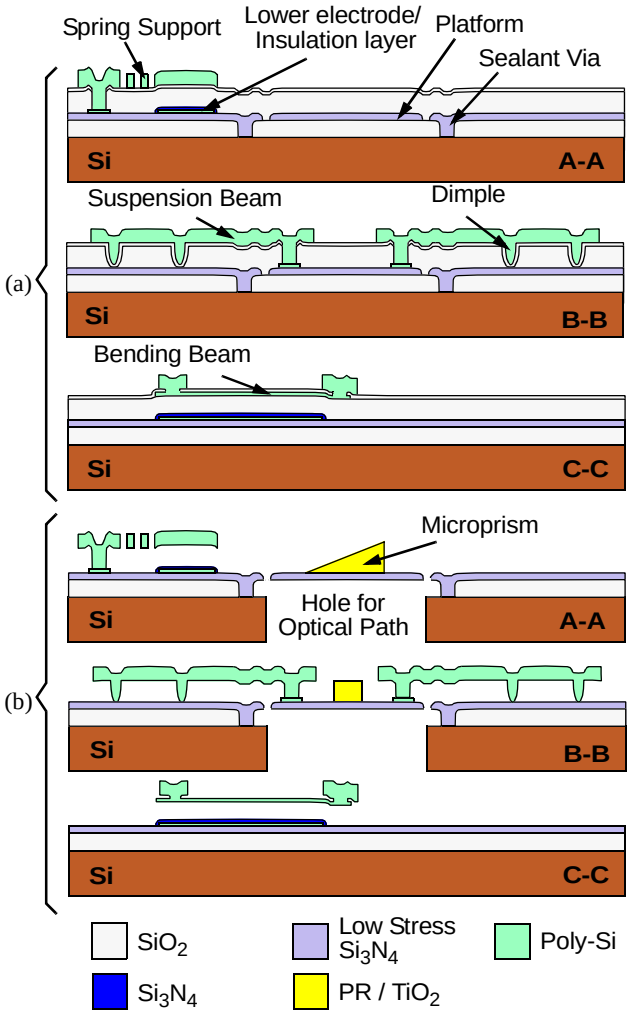

Fig. 4: Cross-sections describing the tiltable microprism process flow at (a) a point just before prism processing; and (b) the end of the process (i.e., final cross-section).

At this juncture, dimple molds are formed by first RIE'ing vias corresponding to dimple locations into the thick sacrificial oxide, then blanket depositing a 1500Å-thick spacer layer of HTO that effectively sets the dimple-to-substrate spacing. This method for forming dimples eliminates the need for the timed etch needed in a previous dimple-formation process [6], and greatly enhances the accuracy to which the dimple-to-substrate gap spacing can be set.

Openings are then etched via RIE into the thin HTO layer above the bending beams and into the thick HTO layer in the field to form attachments between the bending beams and the thicker structural layer making up the platform suspension beams and spring support (c.f., Fig. 2), and to form an anchor to the substrate for the spring support. (Note that this is the only point rigidly attached to the substrate.) The thick structural features are then formed via a 2μm-thick LPCVD, low-stress polysilicon deposition at 588°C, followed by subsequent doping and patterning to form the suspension beams and spring support, and yielding the cross sections of Fig. 4(a).

To form the photoresist microprism on the microplatform, HTO is first removed over the microplatform, and a 2.7μm-thick photoresist layer (AZ1800 series) is spun on. The microprism is then delineated by exposing the photoresist through a gray-scale mask [7] that

Table 1: Bent-Beam Actuated Microplatform Design

Parameter	Value	Units
Microplatform Size	100×90	μm
Bending Beam Length, L_{bb}	94	μm
Bending Beam Width, W_{bb}	18	μm
Bending Beam Thickness, h_{bb}	0.3	μm
Actuation Electrode Length, L_e	83	μm
Dimple Height, h_d	3.45	μm
Electrode Dielectric Thickness, t_{nit}	0.18	μm
Polysilicon Young's Modulus, E	150	GPa

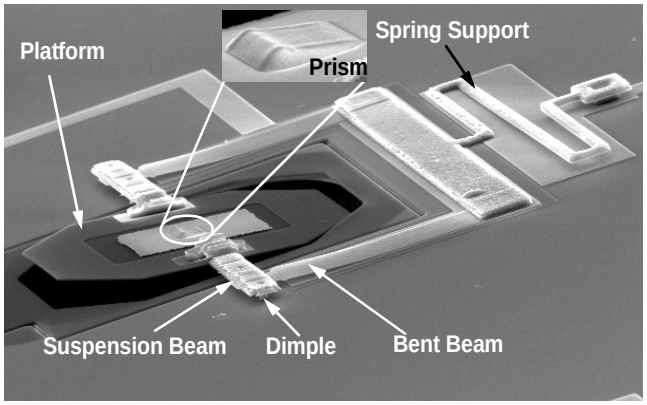

Fig. 5: SEM of a microplatform housing a photoresist microprism with 11V applied actuation voltage. The tilt angle is 7°.

affects a linear variation in exposure intensity over the prism area, effectively exposing a triangular shaped cut into the photoresist thickness. A subsequent development step then removes all exposed photoresist, leaving behind a photoresist microprism.

To allow the passage of light through the microprism, a through-wafer hole is etched from the back side of the wafer using the Bosch process before release. The release etch is finally done using 48.8 wt. % concentrated HF, followed by a supercritical CO_2 drying step to minimize sticking, yielding the cross section of Fig. 4(b), where three levels of suspension—nitride platform, bending beams, and suspension beams—have been achieved in a single planar process.

V. EXPERIMENTAL RESULTS

Bent-beam actuated microplatforms were designed for various actuation voltage ranges using the theory of Section III, then fabricated using the process of Section IV. Table 1 summarizes the design of the device tested for this paper. Figure 5 presents the SEM of a fabricated microplatform housing a photoresist prism under 11V of applied actuation voltage, clearly showing bending of the thin upper beam to achieve a tilt angle of 7°.

Completed microplatforms were tested using three different methods: (1) direct visual observation in air under an optical microscope; (2) observation under an SEM equipped with electrical feedthroughs (c.f., Fig. 5); and for the best accuracy, (3) the optical measurement setup depicted in Fig. 6. In the last of these, the sample under test is mounted on an xyz-stage and a He-Ne (532nm) laser beam is focused on the microplatform using an objective lens with a focal length of 50mm. A microscope is used to align the laser spot to the microplatform (avoiding the prism, for now). The reflection of the laser beam from the platform is projected onto a white screen with a measurement scale, from which the tilt angle of the microplatform can be extracted using trigonometric identities together with the law of reflection. In effect, the position of the laser spot on the screen and the distance between the screen and the

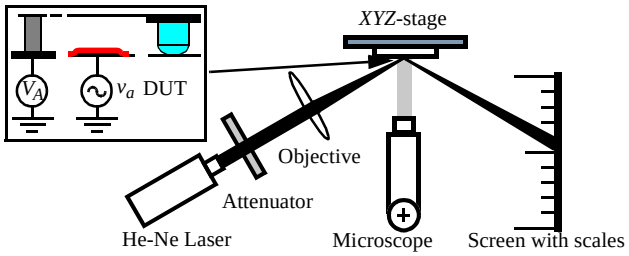

Fig. 6: Test set-up for accurate platform tilt angle measurement.

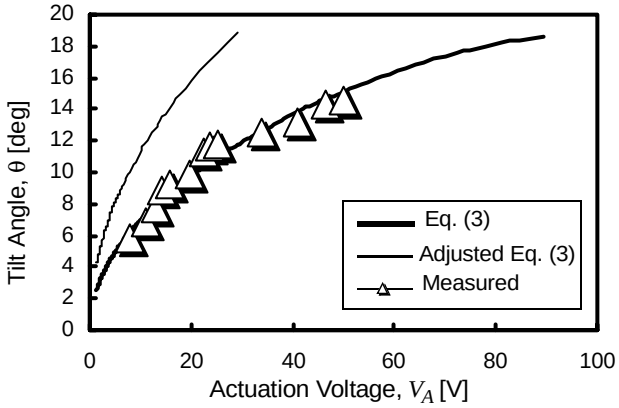

Fig. 7: Measured tilt angle versus actuation voltage for the device of Table 1.

device define the tilting angle.

A. Static Behavior

The fabrication yield of tiltable microplatforms with bent-beam actuators was quite good, with virtually all devices surviving the release and supercritical CO_2 drying steps, including and especially the very thin bending beams. Upon initial testing under an optical microscope, all tested devices were found to be operable with no problems for actuation voltages V_A from 0-20V. However, when voltages exceeded 30V, the bending beams of a small subset of the devices became stuck to their actuation electrodes. Once stuck in this manner, probing could only free bending beams for about half the devices. The other half had bending beams that could be moved laterally by probing (so they weren't fused), but that remained pinned to the actuation electrodes, suggesting charging of the nitride dielectric as a possible cause for the observed sticking.

Figure 7 presents a plot of tilt angle versus actuation voltage for the device of Table 1 as measured using the set-up of Fig. 6. The theoretical prediction of (3) is also plotted in Fig. 7 and is seen to be offset from the measured curve, consistently predicting values lower than measured. This mismatch between theory and measurement is caused by a combination of (1) dimple non-ideality, whereby the dimple is not a perfectly rounded pivot, but in fact has a somewhat flat bottom, so pivots along an edge instead; and (2) the finite width of the platform suspension beams. To account for these non-idealities, the "2" in the numerator of the argument of (3) is changed to "1.22", yielding the adjusted curve shown in Fig. 7, which now very closely matches the measured data.

B. Dynamic Behavior

To characterize the dynamic behavior of the device, frequency spectra were obtained by applying a DC voltage to the bending beam, while applying a swept-frequency AC voltage to the lower electrode (c.f., Fig. 6). As the frequency of the AC voltage increases, the laser spot of Fig. 6 begins to blur into a continuous line, as shown in Fig. 8, and reaches a maximum length at the resonance frequency, at which point the platform/suspension system exhibits its largest vibration amplitude.

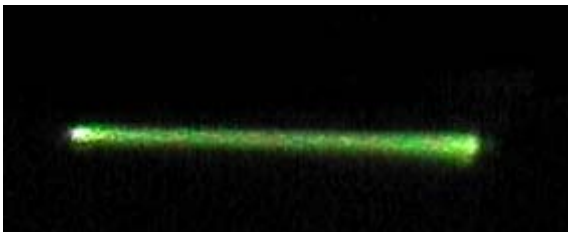

Fig. 8: Reflected laser beam trace during AC measurement.

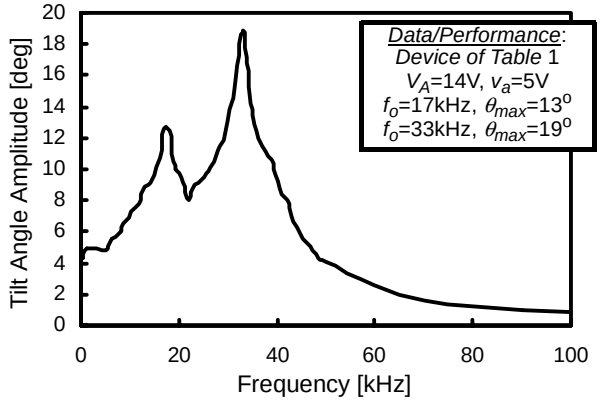

Fig. 9: Measured frequency spectrum of the bent-beam microplatform of Table 1.

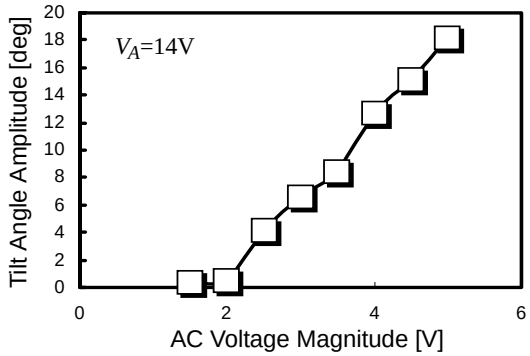

Fig. 10: Tilt angle as a function of AC voltage amplitude for the bent-beam actuated microplatform of Table 1.

Figure 9 presents the measured frequency spectrum for the bent-beam actuated microplatform of Table 1. Here, two resonant peaks are seen, possibly arising from the mechanical filter [8] nature of the overall system, where each of the two bent beams act as resonators coupled loosely by the platform and its suspensions. The lower peak at 17 kHz has a maximum tilt angle around 13°, while the higher peak at 33 kHz has a maximum tilt angle of 19°. Both peak frequencies are quite high compared with frequencies achieved by alternative tilt actuation mechanisms, making bent-beam actuation a strong candidate for high speed optical applications. As expected, the voltages required to tilt at such angles at resonance are much smaller than those needed in static operation. Figure 10 presents a measured plot of tilt angle versus AC voltage amplitude for the device of Table 1 under a constant DC voltage V_A of 14V, showing actuation voltages for this bent-beam actuation method much smaller than for alternative methods.

Figure 11 finally presents measured curves of resonance frequency and resonance tilt angle versus DC bias. Here, an expected strong dependence of resonance tilt angle on DC bias is exhibited. On the other hand, only a weak dependence of resonance frequency on DC bias is observed, which for the higher frequency peak actually increases with DC-bias, suggesting that suspended bending beam length reductions by pinning are slightly more important than

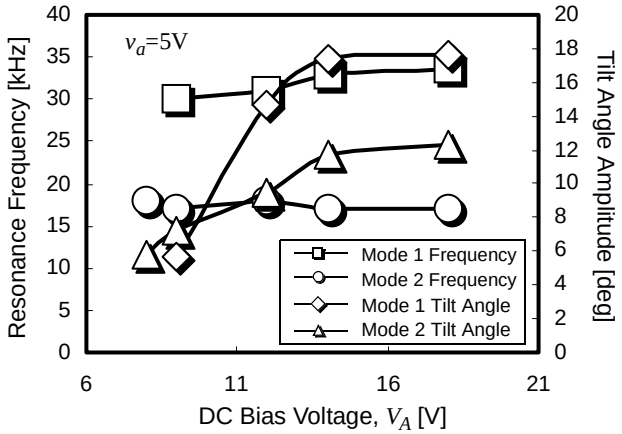

Fig. 11: Resonance frequency and tilt angle as a function of DC voltage for each mode of the device in Table 1.

electrical spring softening [6] for this peak.

VI. CONCLUSIONS

An electrostatic bent-beam actuated tiltable microplatform fabricated using a combined surface micromachining and deep RIE technology has been demonstrated with a measured maximum tilt angle and resonance frequency of 19° and 33 kHz, respectively, obtained using a voltage combination of 14V DC and 5V amplitude AC. Given that the described bent-beam actuation technique is largely electrostatic in nature, the tilt angle-to-voltage/power ratio achieved by the above values represents one of the largest available using MEMS technology, and the numbers demonstrated here can even be bettered by reducing bending beam thicknesses. This, combined with an implementation structure conducive to transmission-based optical signal processing, makes bent-beam actuation a good candidate for 3D arrayed adaptive vision applications. In this regard, the tiltable dispersive microprism function of this device is presently under evaluation.

***Acknowledgment*:** This work was supported under an ARO MURI on an Adaptive Optoelectronic Eye.

References.

[1]M.-H. Kiang, *et al*., "Surface-micromachined electrostatic-comb driven scanning micromirrors for barcode scanners", *MEMS'96*, San Diego, Feb. 11-15, 1996, pp. 192-197.

[2]M. E. Motamedi, *et al*., "MOEM scan engine for bar code reading and factory automation", *Proceedings of SPIE*, vol. 3276, *Miniaturized Systems with Micro-Optics and Micromechanics III*, Jan. 24 -30, 1998, San Jose, CA, pp. 66-80.

[3]V. R. Dhuler, *et al*., "A novel two axis actuator for high speed large angular rotation", *Transducers'97*, Chicago, June 16-19, 1997, pp. 327-330.

[4]D. Berwick, *et al*., "A chromaticity space for specularity, illumination color- and illumination pose-invariant 3-D object recognition", *Proceedings*, 6th IEEE Int. Conf. on Computer Vision, Bombay, India, 1998, pp. 165-170.

[5]R. Legtenberg, *et al*., "Electrostatic curved electrode actuators", *JMEMS*, vol. 6, no. 3, pp. 257-265, Sept. 1997.

[6]K. Wang, *et al.*, "VHF free–free beam high-*Q* micromechanical resonators", *JMEMS*, vol. 9, no. 3, pp. 347-360, Sept. 2000.

[7]W. Daschner, *et al*., "General aspheric refractive micro-optics fabricated by optical lithography using a high energy beam sensitive glass gray-level mask", *J. Vac. Sci. Technol.* B 14(6), pp. 3730-3733, Nov./Dec. 1996.

[8]R. A. Johnson, *Mechanical Filters in Electronics*. New York: Wiley, 1983.